ELSEVIER

Journal of Magnetism and Magnetic Materials 191 (1999) 261–276

Journal of magnetism and magnetic materials

Magnetic ordering of $ErFe_4Ge_2$ studied by neutron diffraction and magnetic measurements

P. Schobinger-Papamantellos[a,*], J. Rodríguez-Carvajal[b], G. André[b], C.H. de Groot[c], F.R. de Boer[c], K.H.J. Buschow[c]

[a]*Laboratorium für Kristallographie, ETHZ CH-8092 Zürich, Switzerland*
[b]*Laboratoire Leon Brillouin, (CEA-CNRS) Saclay 91191 Gif sur Yvette Cedex, France*
[c]*Van der Waals-Zeeman Institute, University of Amsterdam, NL-1018 XE Amsterdam, Netherlands*

Received 25 June 1998

Abstract

The magnetic properties of the compound $ErFe_4Ge_2$ have been studied by magnetic measurements and neutron diffraction. Magnetic ordering was found to set in below $T_N = 42$ K. Magnetic ordering is accompanied by an orthorhombic deformation of the tetragonal lattice, starting at about 35 K. At 8 K there is a further phase transition characterised by a spin-reorientation of the Er moments. The magnetic structure at 1.5 K consists of a canted arrangement with three-dimensional components and two different Er sites. The moment of Er1 equals 5.4(1) μ_B and makes an angle of 55°(2°) with the *c*-axis, while the moment of Er2 equals 8.5(2) μ_B and makes an angle of 42°(2°) with the same axis. The Fe moment ordering displays a three-dimensional canting.

PACS: 74.25.Ha; 75.20.En; 75.25. +z; 75.30. − m; 75.50.Ee; 76.30 Kg

Keywords: Rare earth compounds; Neutron diffraction; Crystal structure; Magnetic structure; Magnetostriction

1. Introduction

Ternary rare earth compounds of the formula RFe_4Ge_2 where R = Y, Dy, Er, Lu crystallise with the $ZrFe_4Si_2$-type of structure [1] (space group, $P4_2/mnm$, $a = 0.7004$ nm $c = 0.3755$ nm, $Z = 2$). In this structure type, the Zr atoms occupy the 2(b) site at (0, 0, 1/2), the Fe atoms occupy the 8(i) site at (0.092, 0.346, 0) and the Ge atoms the 4(g) site at (0.2201, − 0.2201, 0). The RFe_4Ge_2 compounds were reported to order ferromagnetically at very elevated temperatures, T_C varying between 963 and 643 K for R = Y and Lu, respectively [2]. However, these results could not be confirmed in a later ^{57}Fe Mössbauer study of $DyFe_4Ge_2$ that showed no magnetic ordering to be present above about 65 K [3]. Furthermore, magnetisation measurements made at 4.2 K on the same compound showed the absence of a net magnetic moment in the low-field region, indicating an antiferromagnetic moment arrangement of both sublattices if both would order. Field-induced moments were observed even though in the high-field part of the

* Corresponding author. Tel.: 1-632-3773; fax: 1-632-1133; e-mail: nelly@kristall.erdw.ethz.ch.

0304-8853/99/$ – see front matter
PII: S0304-8853(98)00350-3

4.2 K isotherm, presenting magnetisation jumps at 1.6 and 6.0 T, with an ultimate moment of about 8 μ_B/f.u. reached at 35 T [3]. Preliminary magnetisation measurements made by us on several other compounds of the same series indicated that their magnetic behaviour is qualitatively the same as that reported for $DyFe_4Ge_2$.

From the bulk properties alone it is impossible to find a model able to describe the ordering of the two magnetic sublattices. The latter might be quite complex, especially if the magnetic ordering of both sublattices involves competing anisotropies. Nevertheless, the results of magnetisation measurements and Mössbauer spectroscopy allow some conclusions to be drawn: (i) The ferromagnetic ordering reported in Ref. [2] is most likely associated with an Fe impurity. (ii) If both the Fe and the R(Er) sublattices are magnetically ordered at 4.2 K, both moment arrangements are antiferromagnetic and loosely coupled.

For explaining the magnetic behaviour the knowledge of the low-temperature magnetic structures and their temperature dependent evolution are of primary importance, which led us to perform a neutron diffraction study on a representative member of this interesting series of compounds.

2. Sample preparation and magnetic measurements

The $ErFe_4Ge_2$ sample used for neutron diffraction was prepared by arc melting starting materials of at least 99% purity. The sample was wrapped in Ta foil and annealed at 900°C for four weeks in an evacuated quartz tube. After vacuum annealing, the sample was investigated by X-ray diffraction and apart from the main phase of the $ZrFe_4Si_2$-type, was found to contain some weak contributions of the $ErFe_2Ge_2$ compound ($ThCr_2Si_2$ type I4/mmm).

The magnetic measurements were made in the temperature range 5–100 K on a SQUID magnetometer. The temperature dependence of the magnetisation measured in 0.1 T is shown in Fig. 1. This temperature dependence indicates that the magnetic ordering in $ErFe_4Ge_2$ is fairly complicated and involves several steps. With decreasing temperature one observes a somewhat enhanced increase of the magnetisation slightly above 20 K and slightly above 10 K. The low values of the

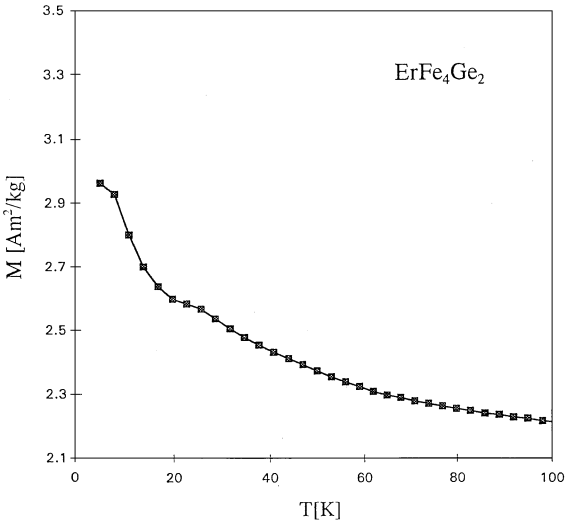

Fig. 1. Temperature dependence of the magnetisation of $ErFe_4Ge_2$ measured in 0.1 T.

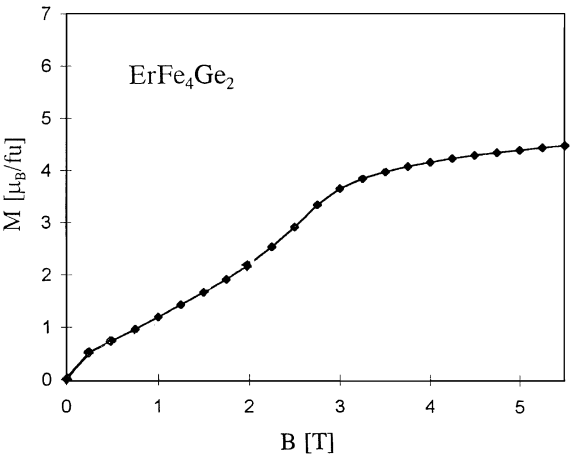

Fig. 2. Field-dependence of the magnetisation of $ErFe_4Ge_2$ measured at 4.2 K.

magnetisation in the whole temperature range considered indicates that the magnetic ordering involves several magnetic sublattices of which the contribution to the overall magnetisation largely cancel. This view is confirmed by the behaviour of the field-dependence of the magnetisation at 4.2 K displayed in Fig. 2, showing that a spontaneous moment is virtually absent. The strong jump of the magnetisation at about 2 T indicates that at this field strength at least some of the antiparallel

moment alignments can be broken. At the highest field strength the magnetisation corresponds to about 5 μ_B per formula unit. This is still far below the value of 13 μ_B expected for Er moments (the free ion value is 9 μ_B) aligned parallel to the Fe moments (0.5 μ_B per Fe atom, as derived from Mössbauer spectroscopy on the isotypic compound $DyFe_4Ge_2$ [3]).

3. Neutron diffraction

Neutron diffraction experiments were carried out in the temperature range 1.5–50 K at the facilities of the Orphée reactor (LLB-Saclay). The data were collected on the G4.1(800-cell position sensitive detector: PSD) and G42 (high resolution: HR 70 detectors with Soller collimators) diffractometers using the wavelengths of 2.426 and 2.3433 Å, respectively. The step increment in 2 θ was 0.1°. The G4.1 data were collected in the 2 θ region 3–83° for a full set of temperatures in the range 1.5–44 K in steps of 2 K. The HR G42 data which extend from 3 to 160° were collected for some selected temperatures in the range 1.5–42 K in steps of 5 K for structural refinements. The data were analysed with the program FullProf [4].

3.1. Crystal structure at 42 K (HR G42 data)

The HR neutron diffraction pattern collected in the paramagnetic state at 42 K, is shown in Fig. 3. The refined parameters and *R*-factors ($R_n = 3.4\%$, $R_{wp} = 11.5\%$) given in Table 1 confirm the $ZrFe_4Si_2$-type of structure [1]. In Table 1 the atomic coordinates are alternatively given in the Cmmm ($\boldsymbol{a}_t\sqrt{2}, \boldsymbol{a}_t\sqrt{2}, \boldsymbol{c}_t$) space group which is a subgroup of order two of the $P4_2/mnm$ space group because $ErFe_4Ge_2$ undergoes a structural transition below $T_N = 42$ K, when magnetic ordering sets in, although the simultaneity of the two (structural and magnetic) orderings have to be confirmed. This facilitates the comparison with the low-temperature refinements. The powder pattern contains a small amount of an unidentified non-overlapping impurity phase that has been excluded from the refinement and is denoted by (i) in Fig. 3.

3.2. Magnetic satellites (G4.1 data)

Some characteristic neutron difference diffraction (G4.1) patterns obtained by subtracting the 40 K paramagnetic state intensities from those of the magnetically ordered region are displayed in Fig. 4. In good agreement with the magnetic measurements magnetic order sets in below $T_N = 42$ K. A large number of magnetic reflections appear in the low angle region of the neutron patterns. All magnetic peaks are situated at reciprocal lattice positions other than those of the nuclear reflections. From all these data and the thermal variation (see next section) of several integrated magnetic intensity lines it can be said that

(i) No ferromagnetism is present.

(ii) The positions of the magnetic reflections remain unchanged in the region 1.5–20 K where the first peak identified as $000 \pm \boldsymbol{q}_1$ (see below) starts to shift to higher 2 θ values.

(iii) The thermal evolution of the magnetic intensities indicates the presence of competing interactions where at least two wave vectors might participate.

The first two peaks within the first Brillouin zone (occurring at 2 θ values of 3.4 and 6.7° were found to be located at reciprocal lattice positions $000 \pm \boldsymbol{q}_i$ with $\boldsymbol{q}_1 \approx (1/8, 1/8, 0)$ and $\boldsymbol{q}_2 = (1/4, 1/4, 0)$, respectively. Using the wave vector $\boldsymbol{q}_2$ we have been able to index all magnetic lines present at all temperatures as satellites of the P cell. Contrary, the exact value of the wave vector $\boldsymbol{q}_1$ could not be refined due to the limited number and the very low intensities of these satellites. Assuming the commensurate value $\boldsymbol{q}_1 = (1/8, 1/8, 0)$ the smallest possible commensurate cell has the dimensions ($\sqrt{2}\boldsymbol{a}, 4\sqrt{2}\boldsymbol{a}, \boldsymbol{c}$), which corresponds to an eightfold cell enlargement.

3.3. Thermal behaviour of magnetic intensities (G4.1 data)

The thermal behaviour of a large number of magnetic reflection lines is shown in more detail in Fig. 5. Magnetic reflection lines appear below $T_N = 42$ K.

The majority of the $\boldsymbol{q}_2$ magnetic satellites and the $000 \pm \boldsymbol{q}_1$ satellite show a non-typical Brillouin behaviour with temperature, most likely because the magnetic structure factors comprise contributions

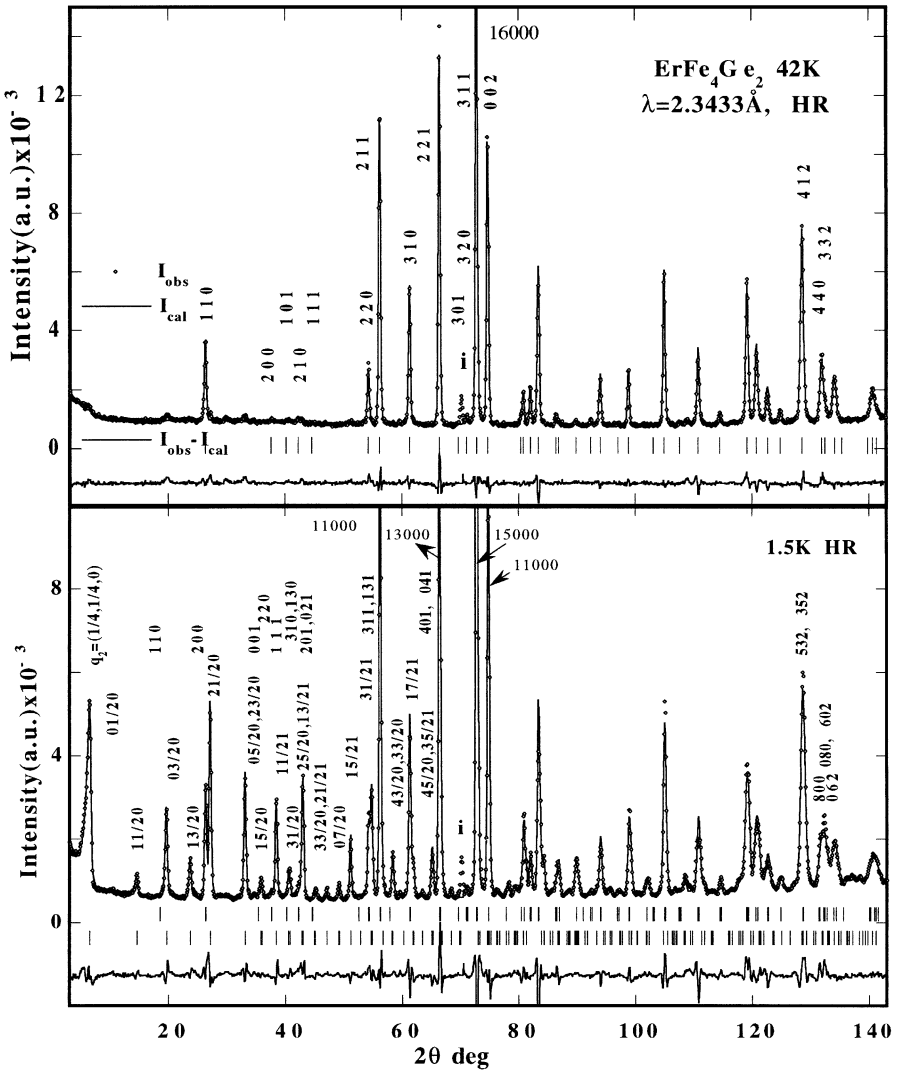

Fig. 3. Observed and calculated neutron intensities of $ErFe_4Ge_2$ (a) in the paramagnetic state at 42 K (top part) (b) in the magnetically ordered region at 1.5 K (bottom). The indexing of the magnetic lines refers to the enlarged orthorhombic cell ($a_t\sqrt{2}$, $2a_t\sqrt{2}$, c). The label (i) indicates unidentified secondary phase. High-resolution data G42 diffractometer.

of two sublattices with competing interactions. In most cases more than one discontinuity or slope change of the magnetic intensities could be observed below T_N. This is for instance the case at $T_1 = 8$ K and $T_2 = 24$ K. These two temperatures correspond roughly to the temperatures at which the magnetisation was observed to increase slightly, as shown in Fig. 1. More pronounced anomalies close to these temperatures were recently reported for the temperature dependence of magnetisation and resistivity as obtained by Canepa et al. [5].

The behaviour of satellites with wave $\boldsymbol{q}_2 = (1/4, 1/4, 0)$ can be better described when one considers two kinds of satellites. The first kind concerns the dominating satellites which are those of the allowed nuclear reflections of the space group like $000 \pm \boldsymbol{q}_2$ and $110 - \boldsymbol{q}_2$. Their presence characterises the entire magnetically ordered regime. As

Table 1

Refined structural parameters of $ErFe_4Ge_2$ from neutron high-resolution data in the paramagnetic state at 42 K and the magnetically ordered state at 1.5 K. For the 42 K data the calculations refer to the tetragonal space group $P4_2/mnm$. For the same temperature the ideal coordinates are also given for the orthorhombic space group Cmmm, so that a comparison can be made with the low-temperature data. For the 1.5 K data the b_0 parameter is divided by 2. The primed labels 1′–4′ in the fifth column denote the coordinates of the four Fe orbits in the magnetically ordered state (see also Table 2). The overall temperature factor equals $B_{of} = 0.0108(5)\,(nm)^2$

$P4_2/mnm$ Atom/site		$P4_2/mnm$ 42 K x	y	z	Cmmm Atom site	Cmmm 42 K x	y	z	Cmmm 1.5 K x	$2y$	z
Er: 2(b)	1	0	0	1/2	Er1: 2(d)	0	0	1/2	0	0	1/2
	2	1/2	1/2	0	Er2: 2(b)	1/2	0	1/2	1/2	0	0
Fe: 8(i)	$(x, y, 0)$	0.0893(2)	0.3546(2)	0	Fe1: 8(p)	x	y	0			
	7	0.3546	0.0893	0	1′	0.13265	0.22195	0	0.1342(7)	0.2234(6)	0
	8	0.6454	−0.0893	0	2′	0.36735	0.27805	0	0.3658(8)	0.2768(6)	0
					Fe2: 8(q)	x	y	1/2			
	5	0.4107	−0.1454	1/2	3′	0.27805	0.13265	1/2	0.2801(6)	0.1310(8)	1/2
	6	0.5893	0.1454	1/2	4′	0.22195	0.3672	1/2	0.2199(6)	0.3688(8)	1/2
Ge: 4(g)	$(x, -x, 0)$	0.2153(3)	−0.2153(3)	0	Ge1: 4 (g)	0.2153	0	0	0.213(1)	0	0
	4	0.2847	0.2847	1/2	Ge2: 4 (j)	0	0.2847	1/2	0	0.14	
a, b (nm), a/b		0.72547(1)	0.72547(1)	1		1.02597	1.02597		1.02753(3)	1.02501(2)	1.002
c(nm)		0.38577(1)				0.38577			0.38554(1)		
R_n(%),		3.4							2.9		
R_{wp}(%)R_{exp}(%)		11.5, 6.5							14.1, 3.98		

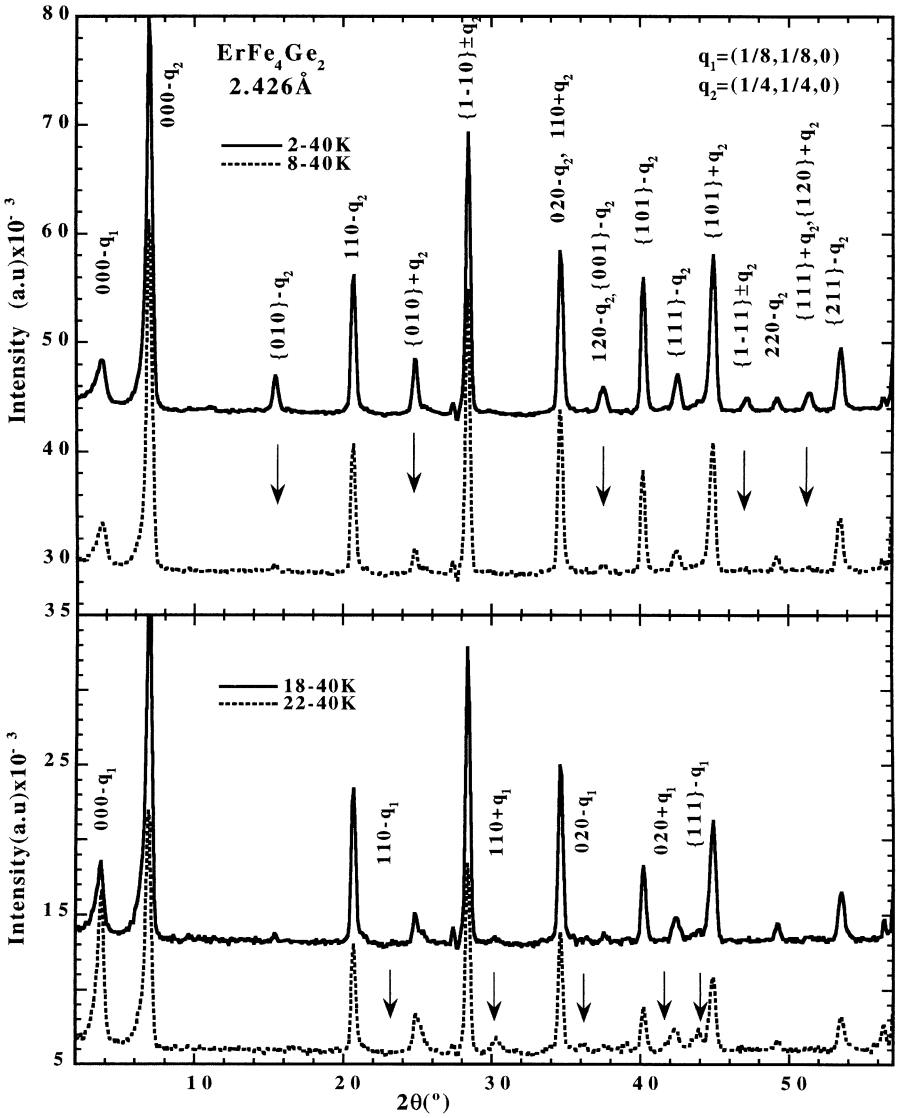

Fig. 4. Neutron difference patterns of $ErFe_4Ge_2$ collected for temperatures above and below the transition temperature $T_1 = 8$ K (top part) and $T_2 = 20$ K (bottom part) indicating the presence of competing interactions (data: G4.1 diffractometer).

shown in the top part of Fig. 5, their intensities are only slightly modified at T_1 but drop abruptly at T_2 and disappear just at $T_N = 42$ K.

The second kind of $\pm\boldsymbol{q}_2$ satellites denoted by arrows in Fig. 4 (top part) are those associated with nuclear reflections of the P lattice but not allowed by the space group applicable to the Er sublattice (0 1 0), $\{1\,2\,0\}/0\,0\,1$ and $\{1\ -1\ 1\}$. These reflections experience the strongest change at $T_1 = 8$ K and some of them vanish for $T \geqslant T_2 = 24$ K while some others display a re-entrant behaviour increasing up to T_2 and decreasing above T_2. This can also be understood if a satellite of the second wave vector incidentally appears at this position. The transition at T_2 is tidily connected with the increase of the $000 \pm \boldsymbol{q}_1$ satellite, see Figs. 4 and 5 (bottom part).

The satellites of the wave vector $\boldsymbol{q}_1$ are much weaker than those of the vector $\boldsymbol{q}_2$ over the whole low-temperature region $1.5\,\mathrm{K} - T_2$. The temperature dependence of the intensity of the most

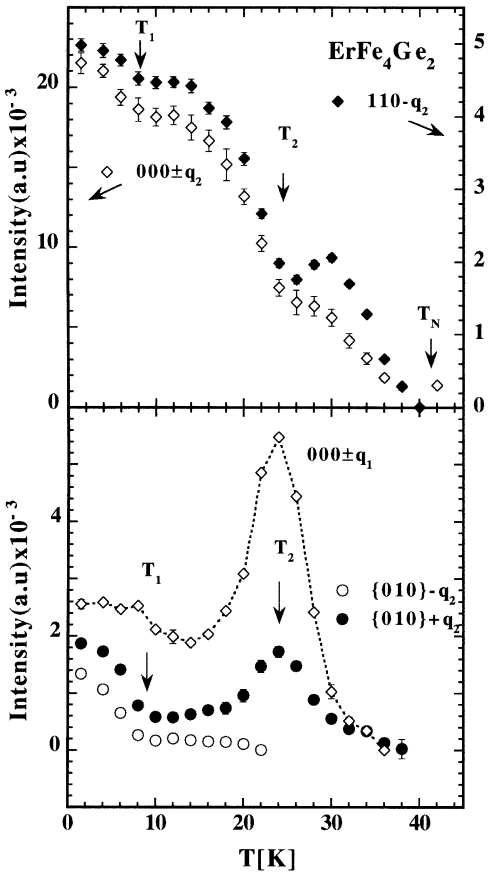

Fig. 5. Characteristic temperature variation of some integrated neutron magnetic intensities pertaining to the wave vector $\boldsymbol{q}_2 = (1/4, 1/4, 0)$ (top part) showing the presence of several transitions. Also shown is the variation of the $000 \pm \boldsymbol{q}_1 \approx (1/8, 1/8, 0)$ satellite (bottom part) and its correlation to the $\boldsymbol{q}_2$ weak set of satellites.

dominant one, $000 \pm \boldsymbol{q}_1$ at $2\theta = 3.4°$, displays only a minor change at $T_1 = 8$ K. It becomes more important in the high-temperature regime, $T > 20$ K, where the intensity ratio $I_{000\pm\boldsymbol{q}_1}/I_{000\pm\boldsymbol{q}_2}$ increases from a value below 0.16–0.66 between 18 and 24 K but drops somehow faster to zero when approaching T_N. The enhancement of the other very weak $\pm\boldsymbol{q}_1$ satellites (denoted by arrows in Fig. 4b) becomes also visible at 22 K and reaches its maximal value at 24 K, cf. Fig. 5. This behaviour indicates the existence of a complex ordering mechanism. If one assumes that both wave vectors contribute to a single magnetic phase one may envisage the existence of two order parameters whose ratio varies with temperature in terms of domains.

Anticipating the results given in the next sections we note that the thermal behaviour of the $000 \pm \boldsymbol{q}_1$ satellite, which is only visible in the G4.1 patterns, bears a resemblance to the behaviour of some nuclear reflections at high angles which indicates a structural phase transition. This transition possibly leads to an incommensurate phase (to be verified) with an orthorhombic average structure which is mainly stable between 24 and 35 K. This fact makes even the nature of $\boldsymbol{q}_1$ questionable and for this reason the present paper will focus on the data analysis of the low-temperature region.

3.4. The low-temperature magnetic structure $\boldsymbol{q}_2 = (1/4, 1/4, 0)$; HR G4.2 data

From the thermal behaviour of the magnetic satellites pertaining to the wave vectors $\boldsymbol{q}_1$ and $\boldsymbol{q}_2$ one may draw the conclusion that in the low-temperature region $T < 20$ K in a first approximation the satellites of the wave vector $\boldsymbol{q}_1 \approx (1/8, 1/8, 0)$ can be neglected since only the $(000 \pm \boldsymbol{q}_1)$ satellite is visible and is about 10 times weaker than the $000 \pm \boldsymbol{q}_2$ satellite.

3.4.1. Symmetry considerations

The star of the wave vector $\boldsymbol{k}_{10} = (x, x, 0)$ has four arms [6]. The symmetry operations of the group $P4_2/mnm$ that leave the wave vector arm $(1/4, 1/4, 0)$ invariant are $G_k = \{E, m_z, m_{xxz}, 2_{xx}0\}$. Symmetry analysis leads to a splitting of the Er site 2(b) into two sites and a splitting of the Fe site 8(i) into four sites, as listed in Table 2. The moments of these six sites (orbits) may have different values and directions. Atoms belonging to the same orbit may have the same moment value and their moment direction is related by symmetry.

Due to their high-symmetry position, the direction of the Er moments is constrained to the mirror plane m_{xxz} (or m_{x-xz} for the arm $(-1/4, 1/4, 0)$). The Er atoms may have either two components parallel to the plane which becomes an antimirror plane m'_{xxz} or a single-moment component which is perpendicular to it (mirror plane m_{xxz}).

Each of the four Fe sites comprises two atoms related by the mirror operation across the plane

Table 2
The splitting of the Er 2(b) site into the I_{Er} and II_{Er} sites and of the Fe 8(i) site into the sites I_{Fe}, II_{Fe}, III_{Fe}, IV_{Fe} caused by the action of the wave vector $(x, x, 0)$ in the parameter space of the $P4_2/mnm$ space group. The labeling of the atoms corresponds to that of Fig. 6

Site/atom	No.	$(x\ y\ z)$	No.	$(x\ y\ z)$
I_{Er}	1	(0 0 1/2)		
II_{Er}	2	(1/2 1/2 0)		
I_{Fe}	1	$(x\ y\ 0)$	7	$(y\ x\ 0)$
II_{Fe}	2	$(-x\ -y\ 0)$	8	$(-y\ -x\ 0)$
III_{Fe}	3	$(-y+1/2\ x+1/2\ 1/2)$	6	$(x+1/2\ -y+1/2\ 1/2)$
IV_{Fe}	4	$(y+1/2\ -x+1/2\ 1/2)$	5	$(-x+1/2\ y+1/2\ 1/2)$

m_{xxz}. The moment components of the atom pairs belonging to the same orbit are symmetry related. For instance the atoms 1,7 of the I_{Fe} orbit have the same moment components parallel to the antimirror plane m'_{xxz} but opposite signs for the component perpendicular to that plane. Thus, the number of free parameters may vary between 14 and 16 (2–4 for the split Er sites and 12 for the split Fe sites). In the low-temperature region where $\boldsymbol{q}_2 = (1/4, 1/4, 0)$ one may carry out the calculations in the enlarged cell $(4\boldsymbol{a}, 4\boldsymbol{b}, \boldsymbol{c})$ or in the four times larger orthorhombic cell $(\boldsymbol{a}_t\sqrt{2}, 2\boldsymbol{a}_t\sqrt{2}, \boldsymbol{c}_t)$ where (0, 1/2, 0) is an antitranslation (P_b lattice). This is illustrated also in Fig. 6. The relation between the two cells and the coordinates are given by

$$(\boldsymbol{a}_0, \boldsymbol{b}_0, \boldsymbol{c}_0) = (\boldsymbol{a}_t, \boldsymbol{b}_t, \boldsymbol{c}_t)P$$

$$\begin{pmatrix} x_0 \\ y_0 \\ z_0 \end{pmatrix} = Q \begin{pmatrix} x_t \\ y_t \\ z_t \end{pmatrix}, \quad \begin{pmatrix} \boldsymbol{a}_0^* \\ \boldsymbol{b}_0^* \\ \boldsymbol{c}_0^* \end{pmatrix} = Q \begin{pmatrix} \boldsymbol{a}_t^* \\ \boldsymbol{b}_t^* \\ \boldsymbol{c}_t^* \end{pmatrix}, \tag{1}$$

where

$$P = \begin{pmatrix} 1 & 2 & 0 \\ \bar{1} & 2 & 0 \\ 0 & 0 & 1 \end{pmatrix} \tag{2a}$$

$$P^{-1} = Q = \begin{pmatrix} 1/2 & -1/2 & 0 \\ \bar{1}/\bar{4} & 1/4 & 0 \\ 0 & 0 & 1 \end{pmatrix} \tag{2b}$$

The obtained coordinates are $x_0 = (x - y)_t/2$, $y_0 = (x + y)_t/4$, $z_0 = z_t$ (see Table 1).

Once the moment components (Fourier coefficients) within the tetragonal cell are defined the magnetic moment direction of any translationally equivalent atom may be calculated:

The magnetic moment value μ_{nj} of the jth atom in the nth cell at position $\boldsymbol{R}_n$, is given by the relation:

$$\mu_{nj} = \sum_{\{\boldsymbol{q}\}} \boldsymbol{S}_{\boldsymbol{q}j} \exp\{-2\pi i \boldsymbol{q}\boldsymbol{R}_n\}$$

$$= \sum_{1/2\{\boldsymbol{q}\}} [\boldsymbol{R}_{\boldsymbol{q}j} \cos\{2\pi(\boldsymbol{q}\boldsymbol{R}_n + \varphi_{\boldsymbol{q}j})\} + \boldsymbol{I}_{\boldsymbol{q}j} \sin\{2\pi(\boldsymbol{q}\boldsymbol{R}_n + \varphi_{\boldsymbol{q}j})\}], \tag{3}$$

where the general Fourier coefficients are:

$$\boldsymbol{S}_{\boldsymbol{q}j} = 1/2\{\boldsymbol{R}_{\boldsymbol{q}j} + i\boldsymbol{I}_{\boldsymbol{q}j}\} \exp\{-2\pi i \varphi_{\boldsymbol{q}j}\} = \boldsymbol{S}^*_{-\boldsymbol{q}j}. \tag{4}$$

For a sinusoidaly modulated structure (single pair $\boldsymbol{q}$, $-\boldsymbol{q}$ and $\boldsymbol{I}_{\boldsymbol{q}j} = 0, \boldsymbol{R}_{\boldsymbol{q}j} = \mu_{0j}/2\boldsymbol{z}$) this expression is

$$\boldsymbol{\mu}_{nj} = \mu_{0j} z \cos(2\pi \boldsymbol{q}.\boldsymbol{R}_n + \varphi_j), \tag{5}$$

where μ_{0j} is the amplitude of the moment, $\varphi_{\boldsymbol{q}j}$ (or φ_j) is the phase relative to the origin, and $\boldsymbol{z}$ is a unit vector along the moment direction. Translationally equivalent atoms in the enlarged cell have the same moment value but may have different signs. For instance, the sign change $(+\ +\ -\ -)$ of four translationally equivalent Er atoms along $\boldsymbol{a}_t$ or $\boldsymbol{b}_t$ can be achieved by choosing the phase $-\pi/4$ (or $(+\ -\ -\ +)$ for $\pi/4$) for the origin Er atom at (0, 0, 1/2) and by applying Eq. (5) to $\boldsymbol{R}_n$ $(n = 0, 3)$. These relationships can also be verified in Fig. 6.

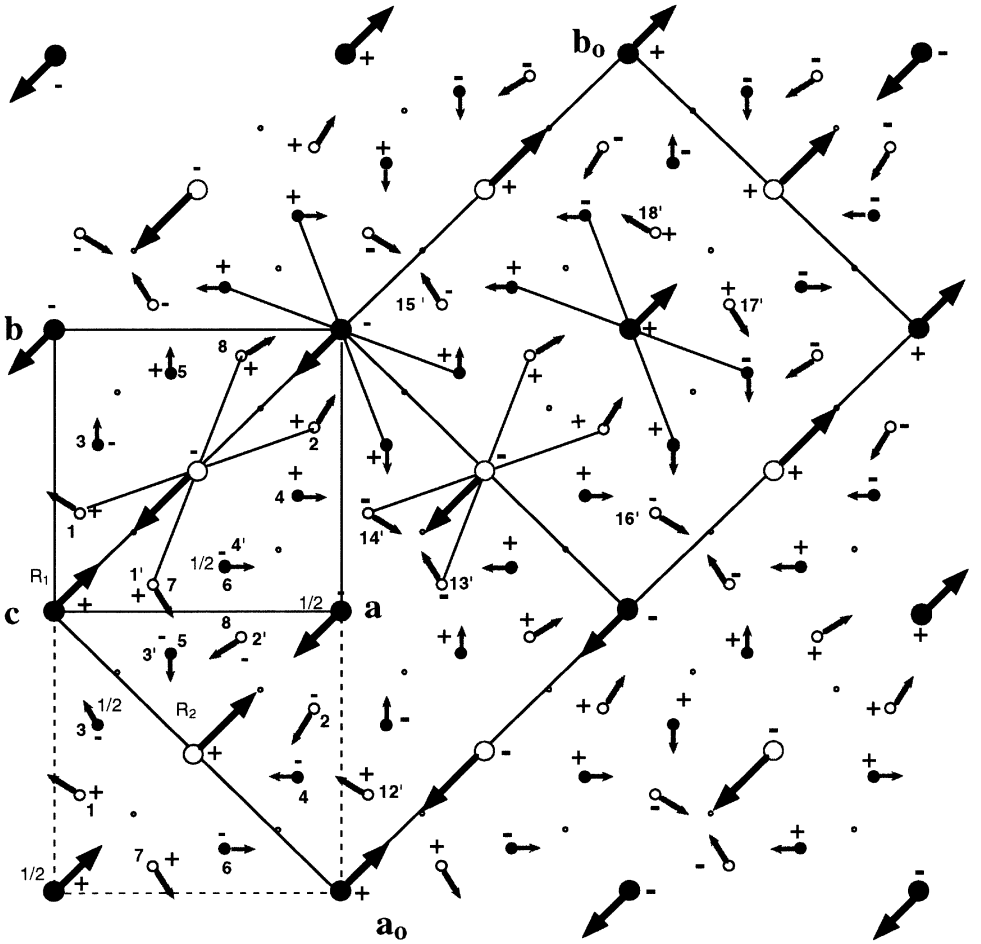

Fig. 6. Schematic representation of the three-dimensional canted magnetic structure of $ErFe_4Ge_2$ at 1.5 K when viewed along [0 0 1].

3.4.2. Orthorhombic structural distortion

In the analysis of the 1.5 K HR neutron data, preference was given to the refinement in the orthorhombic Cmmm enlarged cell instead of the small tetragonal with the wave vector $\boldsymbol{q}_2$. The reason for this was a peak misfit and therefore a very high value of R_{wp}, exceeding 25%, when applying tetragonal symmetry. When the a_0, b_0 parameters of the enlarged cell $(\boldsymbol{a}_t\sqrt{2}, 2\boldsymbol{a}_t\sqrt{2}, \boldsymbol{c}_t)$ are left free to vary one finds that it leads to a reduction of the profile factor to the value 14%. This fact indicates a symmetry reduction when going from the paramagnetic state to below T_N:

$$P4_2/\mathrm{mnm}(T > T_N) \rightarrow \mathrm{Cmmm}(T < T_N). \quad (6)$$

The symmetry reduction occurs at, or close to, the magnetic transition temperature and involves an in-plane deformation of the tetragonal cell.

At 1.5 K, the orthorhombic peak splitting becomes better visible in the high angle region $2\theta > 100^\circ$. The peak half-width of the nuclear reflections (at these angles the magnetic contributions are small) is visibly larger than that in the 42 K data shown in Fig. 3 and is stronger for the $(h\,h\,l)_t$ than for the $(h\,k\,l)_t$ reflections. The transformation of the indices follows that of the lattice constants described in Eq. (2a): $(h_0\,k_0\,l_0) = (h_t\,k_t\,l_t)P$. For the nuclear structure $(\boldsymbol{a}_t\sqrt{2}, \boldsymbol{a}_t\sqrt{2}, \boldsymbol{c}_t)$, each tetragonal peak $(h\,k\,l)_t$ splits into the orthorhombic pair $(h_t - k_t, h_t + k_t, l_t)_0$ and $h_t + k_t, h_t - k_t, l_t)_0$ in the

powder diagram which explains the larger splitting for $h = k$. As can be seen in Table 1, comprising only structural parameters, the ***a***-axis becomes larger and the ***b***-axis becomes smaller than the 42 K values. As this distortion is not large compared with the instrumental resolution, the errors in the atomic positions are larger for the 1.5 K data set. In order to compare the parameter values obtained at 1.5 K to those obtained in the paramagnetic state at 42 K, y is multiplied by a factor of 2 and b_0 divided by a factor of 2 in Table 1. The reliability factors $R_n = 2.9\%$ and $R_{wp} = 14.1\%$ are satisfactory.

3.4.3. The low-temperature magnetic structure, $T < 20$ K

(a) 1.5 K. The refinement of the 1.5 K data has converged for a canted arrangement with three-dimensional components. In view of the large number of free parameters and the tetragonal pseudosymmetry the refinement of powder data is only feasible by inserting parameter constraints. The results given in Table 3 consider two models using different constraints. The best fit is obtained for model I and the corresponding magnetic structure is shown in Fig. 6.

Model I. In this model the moments of the two Er orbits are confined to the $(1\ -1\ 0)_t$ plane or $(1\ 0\ 0)_0$. The moment of Er1 equals 5.4(1) μ_B and makes an angle of 55°(2°) with the ***c***-axis, while the moment of Er2 equals 8.5(2) μ_B and makes an angle of 42°(2°) with the same axis. The Fe ordering has a three-dimensional canting. The four Fe orbits labelled by (1′, 2′, 3′, 4′) in the orthorhombic cell (see Fig. 6) are situated at the corners of an almost regular tetrahedron with very short Fe–Fe distances. The refinement of the Fe moment values became quite unstable when leaving all parameters free (4 × 3). Therefore, a constraint was imposed to the moment values, assuming that the pairs of atoms belonging to orbits (1′, 2′), and (3′, 4′) have the same values of 2.4(2) μ_B and 1.4(2) μ_B Fe atom, respectively. A second constraint was imposed to the angles with the x-axis. The refinement indicated a perpendicular arrangement of the atom pairs (1′, 2′) and (3′, 4′) but invloved a large error. Therefore, the angles were constrained to $\pi/2$. The moments of the four Fe orbits at the corners of the tetrahedron have different space directions indicating an antiferromagnetic interaction.

Within the (x y 0) plane the Er atoms are located in the center of a rectangular oblong with four nearest Fe atom neighbours located at its corners. The Er1 atom which has the lower moment value is surrounded by the III_{Fe} and IV_{Fe} orbits (full circles) which have also the lower moment values. The Er2 atom is surrounded by the I_{Fe} and II_{Fe} orbits (open circles) and has an opposite direction to that of the II_{Fe} moments and a canted to I_{Fe}. As already said the moments of these pairs of Fe sites were constrained to be mutually perpendicular. The refined magnetic canted model at 2 K with the wave vector $\boldsymbol{q}_2$ has only monoclinic symmetry $P_b m'11$. The reliability factors $R_n = 2.9\%$, $R_m = 7\%$ indicate a satisfactory agreement between the model calculations and observations.

Model II. In this model we apply a constraint to the Fe moment values, following results obtained from ^{57}Fe Mössbauer spectroscopy for the $DyFe_4Ge_2$ compound [3]. The spectrum obtained at 8 K suggests that the ordered Fe moments do not exceed the value 0.6(1) μ_B in the latter compound, and a similar moment value is expected therefore also in $ErFe_4Ge_2$ on this basis. The results obtained with this constraint are shown in the third column of Table 3. It is obvious that the agreement between the model calculations and the observed neutron data is less satisfactory. R_m increases from 7% in model I to 11.7% in model II for the same number of free parameters. Furthermore, the Er2 moment value of 9.8(2) μ_B exceeds the free ion value $g\boldsymbol{J}\mu_B 9\ \mu_B$. Therefore, we will only consider model I in the following.

10 K–20 K. The transition starting at 8 K is characterised by an Er moment reorientation. Results are given in Table 3 and in Fig. 7. The refined neutron pattern at 10 K indicates that Er1 has almost the same moment value but rotates towards ***c***, with $\varphi_c = 37°(3°)$. The Er2 moment is slightly reduced but maintains its original orientation with $\varphi_c = 44°(3°)$ within the error limits. Less important changes are visible in the Fe orbits. The moment values of the III_{Fe} and IV_{Fe} orbits surrounding Er2 are also reduced, while the moment values of the I_{Fe} and II_{Fe} orbits surrounding Er1 remain the same. Concerning the angles to the axes, it should

Table 3

Refined magnetic parameters of $ErFe_4Ge_2$ at various temperatures from HR neutron data. μ_x, μ_y, μ_z, μ_T are the moment components the Er and Fe′ sublattices φ_a, φ_c are the moment angles with the $\boldsymbol{a}_o = \sqrt{2}\boldsymbol{a}_t$, $\boldsymbol{c}_o = \boldsymbol{c}_t$ axes. R_n, R_m, are the reliability factors for the integrated intensities of the nuclear and the magnetic structures, respectively. For $T = 1.5$ K in model II the Fe moment values were constraint to the 8 K Moessbauer data 0.6(1) μ_B[3]

$ErFe_4Ge_2$ Cmmm	1.5 K Model I	1.5 K Model II	10 K Model I	20 K Model I	26 K Model I
Er1 at 2(d), (0, 0, 1/2)					
μ_y, $\mu_z[\mu_B]$	4.4(2), 3.1(2)	3.1(2), 3.3(2)	3.4(2), 4.5(4)	2.5(2), 4.6(4)	1.3(11), 2.7(6)
$\mu_T[\mu_B]$, φ_a, $\varphi_c{}^\circ$.	5.4(2), 90, 55(3)	4.5(1), 90, 43(4)	5.6(3), 90, 37(3)	5.2(3), 90, 28(4)	3.0(3), 90, 26(23)
Er2 at 2(b), (1/2, 0, 1/2)					
μ_y, $\mu_z[\mu_B]$	5.7(2), 6.4(3)	6.4 (2), 7.4(2)	4.9(2), 5.1(4)	4.0(1), 4.1(4)	2.6(8), 4.7(7)
$\mu_T[\mu_B]$, φ_a, $\varphi_c{}^\circ$.	8.6(2), 90, 42(2)	9.8(2), 90, 41(1)	7.1(2), 90, 44(3)	5.8(3), 90, 44(3)	5.4(4), 90, 29(10)
Fe1′: (x, y, 0)					
μ_x, μ_y, $\mu_z[\mu_B]$	2.1(1), − 0.5(2), 1.0(2)	0.8(1), − 0.0(2), 0.5(2)	1.4(1), 0.5(1), 0.0(3)	1.3(2), 0.6(2), − 0.1(3)	1.4(4), 0(1), 0.4(5)
μ_T in $[\mu_B]$, φ_a, $\varphi_c{}^\circ$	2.4(2),167(5), − 66(5)	1.00(6), 178(17), − 57(14)	1.5(1), 199(7), − 92(10)	1.4(1), 203(10), − 96(12)	1.4(4), 183(49), − 71(19)
Fe2′: (1/2 − x, 1/4 − y, 0)					
μ_x, μ_y, $\mu_z[\mu_B]$	− 0.3(1), − 1.5(1), − 1.8(2)	− 0.0(2), − 0.7(1), − 0.7(1)	0.4(1), − 1.3(2), − 0.7(2)	0.4(2), − 0.9(3), − 1.0(2)	0.0(5), − 0.6(6), 1.3(5)
$\mu_T[\mu_B]$, φ_a, $\varphi_c{}^\circ$	2.4(2), 257(5), − 220(4)	1.00(6),267(17), − 223(10)	1.5(1), 289(7), − 241(11)	1.4(1), 293(10), − 225(13)	1.4(4),273(49), − 204(29)
Fe3′: (x, y, 1/2)					
μ_x, μ_y, $\mu_z[\mu_B]$	0.7(2), − 0.7(1), − 0.9(1)	− 0.0(2), − 0.7(1), − 0.3(3)	0.3(1), − 0.6(2), − 1.2(1)	0.2(1), − 0.8(3), − 1.0(2)	0.4(6), − 1.2(8), − 1.2(4)
$\mu_T[\mu_B]$, φ_a, $\varphi_c{}^\circ$	1.4(1), − 45(8), 130(9)	0.80(6), − 93(15),110(22)	1.3(1), − 66(8), 151(10)	1.4(1), − 78(11),142(13)	1.7(4), − 72(30),134(24)
Fe4′: (1/2 − x, 1/2 − y, 1/2)					
μ_x, μ_y, $\mu_z[\mu_B]$	0.9(1), 0.9(1), − 0.6(1)	0.76(6), − 0.0(2), − 0.1(1)	1.2(1), 0.5(2), − 0.2(1)	1.3(1), 0.3(3), − 0.0(1)	1.6(5), 0.5(8), − 0.2(4)
$\mu_T[\mu_B]$, φ_a, $\varphi_c{}^\circ$	1.4(1), 45(8), 116(4)	0.77(6), − 3(15), 97(9)	1.3(1), 23(8), 98(5)	1.4(1), 12(10), 91(6)	1.7(4), 18(30), 96(11)
a_0, $b_0/2$ (nm)	1.02754(3), 1.02501(2)	1.02743(6), 1.02512(4)	1.02768(2), 1.02443(2)	1.02749(3), 1.02451(2)	1.02723(6), 1.02489(5)
$2(a_0/b_0)$, c_0 (nm)	1.0024, 0.38554(1)	1.0022, 0.38553(1)	1.0032, 0.38541(1)	1.0029, 0.38545(1)	− ,0.38567(2)
$R_n(\%)$, $R_m(\%)$,	2.9, 7.1,	3.0, 11.7	3.7, 10.7,	3.9, 12.0,	6.4, 25,
$R_{wp}(\%)R_{exp}(\%)$	14.1, 3.98	14.6, 3.98	13.5, 5.7	14.5, 5.9	32, 6.7

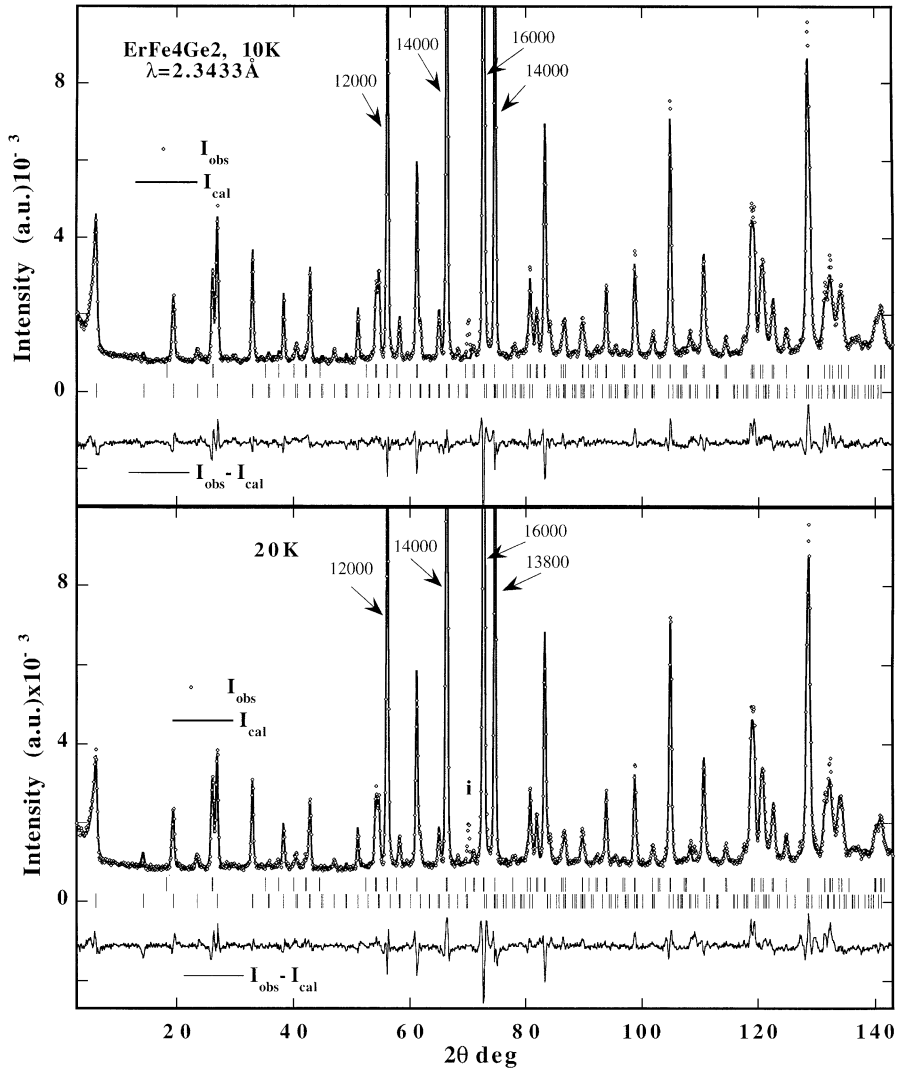

Fig. 7. Observed and calculated neutron intensities of $ErFe_4Ge_2$ in the low-temperature magnetically ordered region at 10 K (top part) and 20 K (bottom part). The peak splitting at high angles is approximated by the orthorhombic distortion. High-resolution data, G42 diffractometer.

be stated that the proposed model fits satisfactorily to the observed intensities but that it should not be considered as unique because of limitations of the powder diffraction. Slight changes in the profile parameters can easily destabilize the refinement and the use of different parameter constraints may produce different canted structures. All that can be said is that no collinear model is able to explain the data. The refined HR data at higher temperatures (15, 20 K) display more important peak misfits which cannot be fully explained by the orthorhombic distortion (see the high-angle region in Fig. 7. This becomes visible in the increasing R_m value (i.e. see data at 20 K in Table 3). The same trend concerning the reorientation of Er1 towards ***c*** and the faster decrease of the Er2 moments is observed also at higher temperatures.

As already mentioned, the magnetic transition is accompanied by large magnetostriction effects. The thermal variation of the a/b ration displayed in

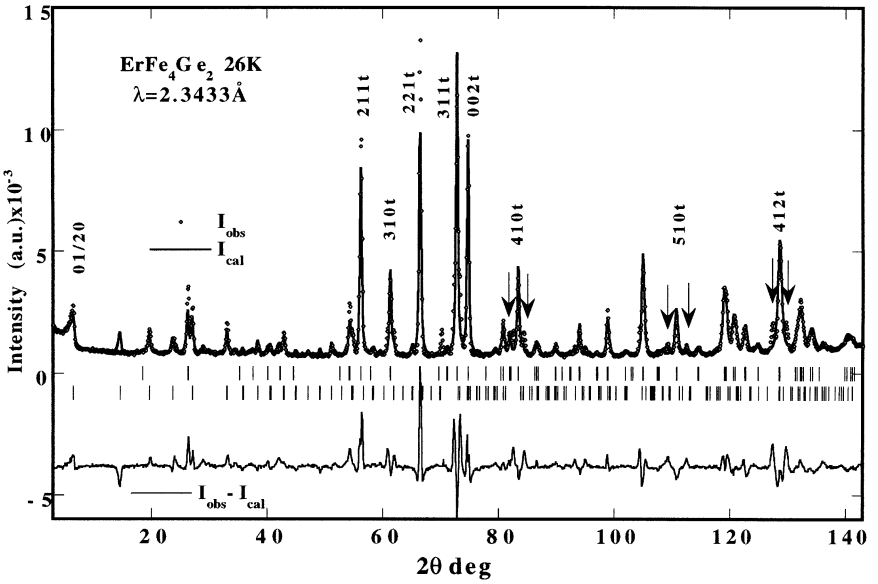

Fig. 8. Observed and calculated neutron intensities of $ErFe_4Ge_2$ in the high-temperature magnetically ordered region at 26 K. The peak splitting at high angles cannot be approximated by the orthorhombic distortion. High-resolution data, G42 diffractometer.

Fig. 10 indicates that the orthorhombic distortion becomes important below 35 K. The thermal variation of this ratio increases linearly to its maximum value at $T_2 = 24$ K and changes its slope twice at lower temperatures.

3.4.4. High-temperature range $20\ K < T_N$

The orthorhombic distortion does not explain all observations above 20 K, in particular when one considers the behaviour of all $h\,h\,l_t$ and $h\,k\,l_t$ nuclear reflections at high angles. Fig. 8 displays the misfit which mainly concerns the dominating nuclear reflections, in particular for the high-angle region in the 26 K data (results are included in Table 3 for comparison). The relative intensities are completely different from those at low temperatures. Around all tetragonal $h\,k\,l_t$ reflections with $h \neq k$ one observes an almost equidistant satellite couple which apparently arises at the cost of the main intensity compared to the 42 K data or to the LT data.

This behaviour is just the opposite of what has been explained for the orthorhombic splitting in Section 3.4.2 and can therefore not be explained by the same mechanism. In Fig. 9 this behaviour is shown on a larger scale for an $h\,k\,l_t$ and an $h\,h\,l_t$ reflection for three temperatures. Just below T_N, i.e. at 35 K, the tetragonal reflection 412_t displays only a minor splitting into the 532_o and 352_o orthorhombic peaks which increases at 20 K. The splitting experienced by $h\,h\,l_t$ reflections is much larger. This behaviour can be described by the increase of the tetragonal angle γ to values larger than 90°. However, there exists a second splitting of the 412_t reflection marked by arrows in the 30 K data. This splitting cannot be explained by a distortion of a second phase with $\gamma_t = 88.2°$ as this is not at all followed by the $h\,h\,l_t$ reflections. This suggests that the HT transition cannot be explained by a mechanism where the tetragonal phase dissociates into two distinct orthorhombic ones with different lattice constants. A further possibility might be that the nuclear structure becomes incommensurate with the crystal lattice. We have been able to make a profile match assuming a three-dimensional modulation. This solution has again the disadvantage that satellites of the low 2θ angle region, such as the satellite $000 \pm \boldsymbol{q}_1$, might be of magnetic origin.

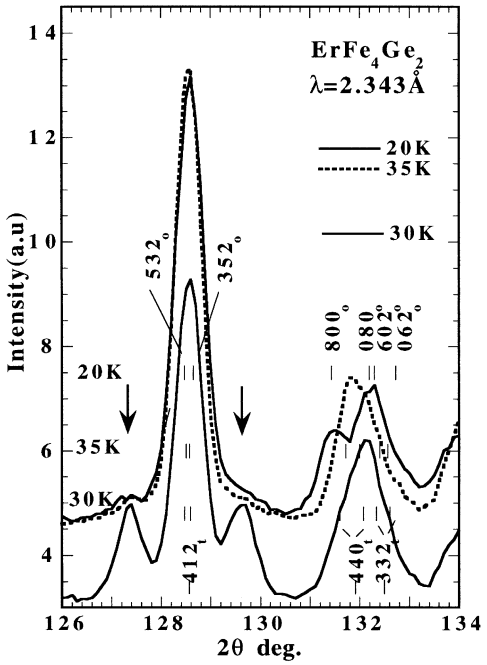

Fig. 9. The splitting of tetragonal $h\,k\,l_t$ and $h\,h\,l_t$ nuclear reflections below the magnetic ordering temperature $T_N = 42$ K associated with the $P4_2/mnm \rightarrow Cmmm$ transition in $ErFe_4Ge_2$ (HR neutron data, $\lambda = 2.343126$ Å). The unexplained satellites of the 412_t reflection marked by arrows disappear below $T = 20$ K while splitting of the $h\,h\,l_t$ reflection becomes more dominant at this temperature.

4. Discussion

We mentioned already in Section 3.4.1 that symmetry analysis of the tetragonal basis structure leads to a splitting of the Er site 2(b) into two sites. Within the (x y 0) planes both types of Er atoms are located in the center of a rectangular oblong with four nearest Fe neighbours located at its corners. This has been indicated in Fig. 6 by the diagonals of the oblong connecting the four Fe neighbours with the central Er atom. In the tetragonal setting, one may derive from Fig. 6 that the orientation of the oblongs centered by Er atoms occurring in adjacent planes (x y 0) planes turns by 90° when going from one plane to the other. This means that also the basal plane component of the crystalline electric field gradient tensor rotates by 90° when moving from one Er plane to the other along the ***c***-direction. However, the exchange interaction between the Er moments is seen in Fig. 6 to lead to an antiferromagnetic structure in which the in-plane components of the Er moments in adjacent planes do not rotate by 90° but remain co-linear. The combination of crystal field and exchange field leads therefore to level schemes for the $(2J + 1)$ manifold that are different for the two Er sites. It follows from the strong difference in moment value for the two Er sites at the lowest temperature considered that the ground states associated with these level schemes are strongly different. Because thermal population of the two-level schemes leads to two different situations one also finds that the thermal behaviour of moment size and direction are strongly different for the two Er sites.

The set of magnetic and nuclear observations suggests the existence of two independent ordering mechanisms operating in this system. This has already been discussed in connection with Fig. 5 but it is clearly shown in Fig. 10 which displays the temperature-dependent behaviour of the lattice constants refined on the basis of the G4.1 data, restricted to only the orthorhombic distortion. In the top part of Fig. 10, one can see that the lattice constant b becomes smaller with decreasing temperature while the a parameter displays just the opposite behaviour.

The non-monotonous behaviour of the a/b ratio shown in the bottom part of Fig. 10 and the magnitude of the corresponding spontaneous strain $\varepsilon_s = e_{xy} \approx |(a - b)/(a + b)|$ suggests that the tetragonal-to-orthorhombic distortion observed in $ErFe_4Ge_2$ may have two different and complementary sources:

1. A structural transition occurring independently from the magnetic order, at a few degrees below T_N (for instance, at 38 K following the a/b curve of Fig. 10). The order parameter of this proper ferroelastic transition [7] is the shear strain e_{xy} associated with $4/mmm \rightarrow m^{xy}mm$ species, in the notation of Ref. [7].
2. A magnetostrictive distortion due to coupling between lattice strains and magnetic properties.

Concentrating on the latter case, based on the many results obtained on rare earth intermetallics it is most likely that a magnetostrictive distortion is

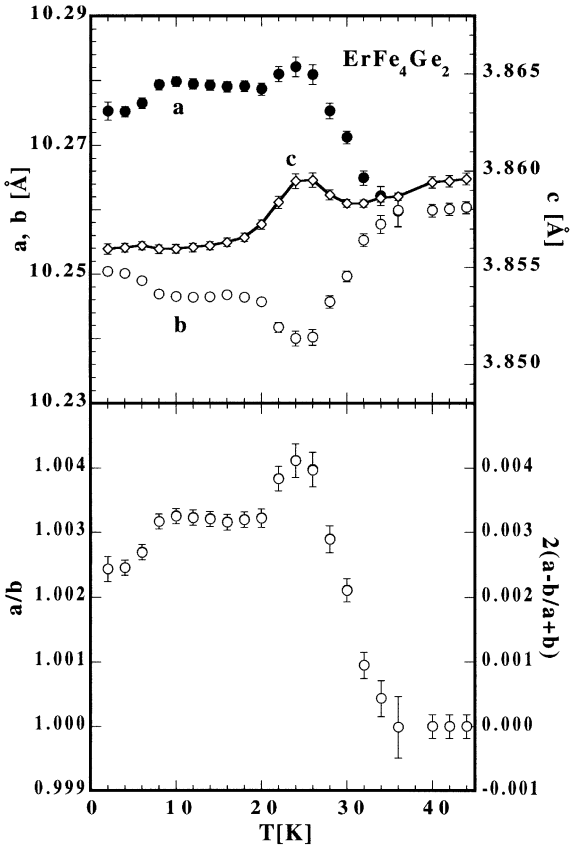

Fig. 10. Top part: Temperature dependence of the lattice parameters $a = a_0$, $b = b_0/2$ and $c = c_0$ as a function of temperature. Bottom part: Temperature dependence of the ratio a/b and $\varepsilon_s = |(a-b)/(a+b)|$. At 35 K these quantities become slightly deviating from the tetragonal case.

associated with the rare earth lattice. But even in this case one has to decide between one-ion and two-ion magneto-elasticity. In the first case, there is a direct coupling between the deformations of the lattice and the 4f shell. In the second case, the magnetoelasticity results from modifications of the two-ion magnetic interactions by the strains.

Somewhat similar phenomena were observed in hexagonal (rhombohedral) rare earth compounds of the type RCo_3 and R_2Co_7 where a strong orthorhombic distortion is observed at low temperatures when the ordered R moments have a basal-plane component (see, for instance Ref. [8] and papers cited therein). The origin of the orthorhombic distortion in these materials is the presence of a sufficiently strong γ-magnetostriction. This γ-magnetostriction is a single-ion property corresponding to a direct coupling between the deformations of the 4f shell and the lattice, and it follows from the discussion given above that the contributions of the Er1 and Er2 sites should be different because of the thermal averages of the involved Stevens operators are different.

More appealing in the present case is a description in terms of two-ion magnetoelasticity in which the magnetic interaction between ions is modified by strains. In fact, in very simple terms one may figure that the dominant R–R exchange interaction has different signs along the $\boldsymbol{a}_o$ and $\boldsymbol{b}_o$ orthorhombic directions. It can easily be seen in Fig. 6 that it is positive along $\boldsymbol{a}_o$ while along $\boldsymbol{b}_o$ it is negative due to the (0, 1/2, 0) antitranslation. These completely different exchange interactions may result in the observed magnetostriction phenomena.

Generally, this situation can be described by a magnetostructural coupling between e_{xy} and the order-parameter η associated with the magnetic ordering and the corresponding symmetry lowering $(4/mmm1' \rightarrow m')$ when going from the paramagnetic to the antiferromagnetic state. This coupling can be shown to be of the form $F(\eta^2, e_{xy}) = \eta^2 e_{xy}$ [9] so that the magnitude of e_{xy} should become affected only for sufficiently large values of η. This may explain the anomalous drop of a/b which occurs below 26 K in Fig. 10. The intensities of the $\boldsymbol{q}_2$ satellites display anomalies around the same temperature as the intensity of the $\boldsymbol{q}_1$ satellite and the lattice constants. Therefore, between these behaviours a correlation might exist, requiring further studies.

Without certitude concerning the nature of the second wave vector, any model choice is questionable. For this reason an independent and systematic study of the nuclear and the magnetic structures is of great value. Synchrotron radiation data with a temperature window of 5° between 2 and 45 K (10 temperatures) would allow to obtain a new entry in this complex matter. Of even more relevance in this connection would be experiments on isotypic RFe_4Ge_2 compounds in which the 4f component has different properties. Such experiments are planned in the near future.

References

[1] Ya.P. Yarmoluk, L.A. Lysenko, E.I. Gladyshevski, Dopovidi Akad. Nauk Ukr., RSR, Ser. A 37 (1975) 279.
[2] O.Ya. Oleksyn, Yu.K. Gorelenko, O.I. Bodak, 10th Int. Conf. on Solid Compounds of Transition Elements, Münster 21–25 May 1991, P-254-FR, SA.
[3] A.M. Mulders, P.C.M. Gubbens, Q.A. Li, F.R. de Boer, K.H.J. Buschow, J. Alloys Comp. 221 (1995) 197.
[4] J. Rodríguez-Carvajal, Physica B 192 (1993) 55. The manual of FullProf can be obtained from a Web browser at ftp://bali.saclay.cea.fr/pub/divers/fullp/doc.
[5] F. Canepa, S. Cirafici, F. Merlo, M. Pani, L. Carpaneto, M.R. Cimberle, J. Alloys Comp. 266 (1998) 26.
[6] O.V. Kovalev, in: H.T. Stokes, D.M. Hatch (Eds.), Representations of the Crystallographic Space Groups, Gordon and Breach, London, 1993.
[7] J.C. Tolédano, P. Tolédano, Phys. Rev. B 21 (1980) 1139.
[8] A.V. Andreev, in: K.H.J. Buschow (Ed.), Magnetic Materials, Vol. 8, Elsevier Science, Amsterdam, 1995, p. 59.
[9] J.C. Tolédano, P. Tolédano, in: The Landau Theory of Phase Transitions, World Scientific, Singapore, 1987.